Solid friction at high sliding velocities : an explicit 3D dynamical SPH approach

C. Maveyraud [1], W. Benz [2], G. Ouillon [1], A. Sornette [1] and D. Sornette [1,3]

[1] LPMC, CNRS UMR6622 and Université de Nice-Sophia Antipolis
B.P. 71, 06108 NICE Cedex 2, France
[2] Physikalisches Institut, Universitaet Bern
Sidlerstrasse 5, CH-3012 Bern, Switzerland
[3] IGPP and ESS department, UCLA, Box 951567
Los Angeles, CA 90095-1567, USA

Abstract: We present realistic 3D numerical simulations of elastic bodies sliding on top of each other in a regime of velocities ranging from meters to tens of meters per second using the so-called Smoothed Particle Hydrodynamics (SPH) method. This allows us to probe intimately the response of the bodies and the nature of the friction between them. Our investigations are restricted to regimes of pressure and roughness where only elastic deformations occur between asperities at the contact surface between the slider block and the substrate. In this regime, solid friction is due to the generation of vibrational radiations which are subsequently escaping to infinity or damped out in which case energy is dissipated. We study periodic commensurate and incommensurate asperities and various types of disordered surfaces. In the elastic regime studied here, we report the evidence of a transition from zero (or non-measurable $\mu < 0.001$) friction to a finite friction as the normal pressure increases above about $10^6\ Pa$. For larger normal pressures (up to $10^9\ Pa$), we find a remarkably universal value for the friction coefficient $\mu \approx 0.06$, which is independent of the internal dissipation strength over three order of magnitudes, and independent of the detailled nature of the slider block-substrate interactions. We find that disorder may either decrease or increase μ due to the competition between two effects: disorder detunes the coherent vibrations of the asperties that occur in the periodic case, leading to weaker acoustic radiation and thus weaker damping. On the other hand, large disorder leads to stronger vibration amplitudes at local asperities and thus stronger damping. Our simulations have confirmed the existence of jumps over steps or asperities of the slider blocks occurring at the largest velocities studied ($10\ m/s$). These jumps lead to chaotic motions similar to the bouncing-ball problem. We find a velocity strengthening with a doubling of the friction coefficient as the velocity increases from $1\ m/s$ to $10\ m/s$. This reflects the increasing strength of vibrational damping.

1 Introduction

Solid friction has a long scientific history, starting probably in the western world about 500 years ago with the work of Leonardo de Vinci, continuing with the empirical Amontons'laws two centuries later and Coulomb's investigations of the influence of slipping velocity on friction in the XVIII century. Only three decades ago was it recognized that friction plays probably a fundamental role in the mechanics of earthquakes [*Brace and Byerlee*, 1966]. Rock mechanicians consider an earthquake as a stick-slip event controlled by the friction properties of the fault, i.e. the destabilization of a weak part of the crust. This formulation has been shaped by laboratory experiments performed under a variety of pressure and temperature conditions (which however reproduce only imperfectly the conditions prevailing in the crust). Numerous laboratory experiments have been carried out to identify the parameters that control solid friction and its stick-slip behavior [*Persson and Tosatti*, 1996]. The most significant variables appear to be the mineralogy, the porosity, the thickness of the gouge, the effective pressure, the temperature and the water content [*Byerlee et al*, 1968; *Brace*, 1972; *Beeman et al.*, 1988; *Gu and Wong*, 1991; *Johansen et al.*, 1993; *Streit*, 1997]. Low velocity experiments have established that solid friction is a function of both the velocity of sliding and of one or several state parameters, roughly quantifying the true surface of contact [*Brace*, 1972; *Dieterich*, 1972; 1978; 1979; 1992; *Ruina*, 1983; *Cox*, 1990; *Beeler et al.*, 1994; 1996; *Baumberger and Gauthier*, 1996; *Scholz*, 1998].

The Ruina-Dieterich laws constitute the basic ingredients in most models and numerical elastodynamic calculations that attempt to understand the characteristics of earthquake sources. A recent lively debate has been whether space-time complexity in earthquake sequences can occur on an homogeneous fault solely from the nonlinear dynamics [*Shaw*, 1993; 1995; 1997; *Cochard and Madariaga*, 1994; 1996] associated with the slip and the velocity dependent friction law [*Dieterich and Kilgore*, 1994; *Dieterich*, 1992], or, does it necessarily require the presence of quenched heterogeneity [*Rice*, 1993; *Benzion and Rice*, 1993; 1995; *Knopoff*, 1996]? It is now understood that complexity can emerge purely from the nonlinear laws but heterogeneity is probably the most important factor dominating the multi-scale complex nature of earthquakes and faulting [*Ouillon et al.*, 1996]. It is also known to control the appearance of self-organized critical behavior in a class of models relevant to the crust [*Sornette et al.*, 1995; *Shnirman and Blanter*, 1998].

A well-known and serious limitation of these calculations based on laboratory friction experiments is that the friction laws have been determined using sliding velocities no more than about 1 cm/s, i.e. orders of magnitude below the sliding velocity of meters or tens of meters believed to occur during earthquakes. The validity of extrapolations, especially the velocity weakening dependence, has yet to be demonstrated. This is all the more relevant when one examines the underlying physical mechanisms giving rise to the friction laws. At low velocity, hysteretic elastic and plastic deformations at the length scale corresponding to asperities seem to play a dominant role [*Bowden and Tabor*, 1954; *Sokoloff*, 1984; *Jensen et al.*, 1993; *Dieterich and Kilgore*, 1994; *Caroli and Nozières*, 1996; *Tanguy and Nozières*, 1996; *Tanguy and Roux*, 1997; *Caroli and Velicky*, 1997; *Bocquet and Jensen*, 1997].

At larger velocities, different mechanisms come into play. Collisions between as-

perities and transfer of momentum between the directions parallel and perpendicular to the motion may become an important mechanism [*Lomnitz*, 1991; *Pisarenko and Mora*, 1994]. This regime is probably relevant to explain the apparent low heat flow and thus low friction coefficient observed along the San Andreas fault, the so-called heat flow paradox. This paradox [*Bullard*, 1954] comes about because, in order to allow for large earthquakes, a fault should have a large friction coefficient so that it can store large amount of elastic energy. However, repeated earthquakes occurring with a large coefficient of dynamical friction should give rise to a significant heat flow at the surface which has not been observed [*Henyey and Wasserburg*, 1971; *Lachenbruch and Sass*, 1980]. One explanation for this low heat flow is that the coefficient of friction is low as a result of dynamical effects affecting the friction during the earthquake. Other possibilities, less explored in the literature, involve fluids [*National Research Council*, 1990] or acoustic vibrations [*Melosh*, 1996]. Several simplified models have recently been explored as possible mechanisms for the generation of a low friction. These mechanisms include crack opening modes of slip [*Brune et al.*, 1993], dynamical collision effects [*Lomnitz*, 1991; *Pisarenko and Mora*, 1994], frictional properties of a granular gouge model under large slip [*Scott*, 1996], space filling bearings with compatible kinematic rotations [*Herrmann et al.*, 1990], hierarchical scaling [*Schmittbuhl et al.*, 1996].

Recently, Tsutsumi and Shimamoto [1996; 1997] have reached a completely novel regime, by performing friction measurements on rotation cylindrical samples at velocities up to 1.8 m/s and for slips of several tens of meters. While these results due to several experimental problems are not completely straight-forward to interpret, they seem to indicate the existence of a change of regime from velocity weakening to velocity strengthening and then again to velocity weakening at the largest velocities. This last regime seems to be associated to the melting of a very thin layer.

The work we report here has been motivated by considerations that different physical mechanisms might lead to a change of regime in the velocity and slip dependence of the solid friction law. Thus, one needs to explore the high velocity regime in as large a variety of conditions as has been done for the low velocity regime. For this purpose, we have developed realistic 3D numerical simulations of elastic bodies sliding on top of each other in a regime of velocities ranging from meters to tens of meters per second. In this way, we probe more intimately than any exprimental setup could do the response of the bodies and the nature of the friction.

We begin by a short presentation of the SPH method and its implementation in our context. We follow by a presentation and a discussion of the results obtained for surfaces with periodic asperities and then with various types of random asperities and conclude.

2 The numerical model

2.1 The SPH method

We have adapted the Lagrangian method called "smoothed particle hydrodynamics" (SPH), initially introduced by Lucy [1977] for hydrodynamic problems with fast dynamics. This method has the avantage of being simple, elegant, easy to implement

and to extend with a reasonable precision. Its most recent improved version makes it well-suited to treat problems with fast moving interfaces. This was our initial motivation to use this property at our advantage to tackle the solid friction problem in the regime of large slipping velocities.

In SPH the physical problem is discretized on a mesh whose nodes, the "particles" are moving or adapting in a Lagrangian manner. Each particles carries with it a set of field variables. An interpolating kernel allows to reconstruct the field variables everywhere by interpolation. Spatial derivatives are obtained from the analytical differentiation of the interpolation kernel. SPH has been used in a variety of applications, such as gas dynamics [*Monaghan and Gingold*, 1983], fragmentation of gas clouds [*Lattanzio et al.*, 1985], radio jets [*Coleman and Bicknell*, 1985], impacts [*Benz et al.*, 1986; *Benz and Asphaug*, 1994; *Benz et al.*, 1994; *Asphaug et al.*, 1998], quasi-incompressible fluid flows [*Monaghan and Humble*, 1993], material rupture [*Benz and Asphaug*, 1995], dam rupture, ocean wave propagation and water falls [*Monaghan*, 1994; 1996]. For reviews, see [*Monaghan*, 1988; 1992; *Benz*, 1990].

2.2 Outline of the approach

Consider one of the physical field $f(\vec{r})$, which is a function of position $\vec{r}$. It can always be written as

$$f(\vec{r}) = \int f(\vec{r}')\ \delta(\vec{r} - \vec{r}')\ d\vec{r}'\ , \tag{1}$$

where δ is the Dirac function. This suggests approximating $f(\vec{r})$ by a smoothing kernel as

$$\langle f(\vec{r}) \rangle = \int f(\vec{r}')\ W(\vec{r} - \vec{r}', h)\ d\vec{r}'\ , \tag{2}$$

$W(\vec{r} - \vec{r}', h)$ is the interpolating kernel and h is the width of the kernel and thus the smoothing scale. The kernel is continuous, differentiable and has the following properties:

$$\int W(\vec{r} - \vec{r}', h)\ d\vec{r}' = 1 \tag{3}$$

and

$$\lim_{h \to 0} W(\vec{r} - \vec{r}', h) = \delta(\vec{r} - \vec{r}')\ . \tag{4}$$

¿From (3) and (4), $\langle f(\vec{r}) \rangle \overset{h \to 0}{\longrightarrow} f(\vec{r})$. From now on, we drop the arrow and write $\vec{r}$ as r, and similarly for the derivatives. For a fluid of density $\rho(r)$, equation (2) reads

$$\langle f(r) \rangle = \int \left[\frac{f(r')}{\rho(r')} \right] W(r - r', h) \rho(r') dr'\ . \tag{5}$$

Discretizing space in N elements of masses m_j, the integral becomes

$$\langle f(r_i) \rangle = \sum_{j=1}^{N} m_j \frac{f_j}{\rho_j} W(r_i - r_j, h)\ , \tag{6}$$

with $f_j \equiv f(r_j)$. Replacing $f(r)$ by $\rho(r)$, this yields the following expression of the fluid density

$$\langle \rho(r_i) \rangle = \sum_{j=1}^{N} m_j W(r_i - r_j, h) \ . \tag{7}$$

This equation has the following interpretation [*Benz*, 1990] : each particle of mass m_j is spatially smoothed out according to the kernel space dependence, which can be seen as its spatial density distribution. The density at any point in space is obtained by summing all contributions from all particles at this point. The term Smoothed Particle Hydrodynamics expresses this interpretation.

The gradient of f is similarly obtained as

$$\langle \nabla f(r) \rangle = \int \nabla f(r') \ W(r - r', h) \ dr' \ . \tag{8}$$

Integrating by parts and using the fact that W goes to zero sufficiently fast so that the surface terms are negligible, one obtains

$$\langle \nabla f(r) \rangle = \int \nabla W(r - r', h) \ f(r') \ dr' \ , \tag{9}$$

with $\nabla W(r - r', h)$ being the gradient with respect to r. Discretizing, this yields

$$\langle \nabla f(r_i) \rangle = \sum_{j=1}^{N} \frac{m_j}{\rho_j} f_j \nabla_i W_{ij} \ , \tag{10}$$

where ∇_i is the gradient with respect to the coordinate of the i-th particle and $W_{ij} \equiv W(r_i - r_j, h)$.

Several choices are possible for the kernel, as long as the conditions (3) and (4) are fulfilled. Kernels constructed on spline functions have several advantages [*Monaghan and Lattanzio*, 1985] :

$$W(r,h) = \frac{1}{\pi h^3} \cdot \begin{cases} 1 - \frac{3}{2}v^2 + \frac{3}{4}v^3 & \text{if } 0 \le v \le 1 \\ \frac{1}{4}(2-v)^3 & \text{if } 1 \le v \le 2 \\ 0 & \text{else,} \end{cases} \tag{11}$$

where $v = \frac{r}{h}$. This kernel has compact support, i.e. interactions between particles vanish for $r > 2h$. Only contributions from neighbors need to be accounted for instead of N^2 contributions. The second derivative of $W(r,h)$ is continuous and the error in the estimation of the interpolation is of order $\mathcal{O}(h^2)$. At the beginning of the calculation, the values of the kernel and its gradient for different values of v are calculated and stored in a array. This allows to decrease the calculation time.

2.3 Equations of motion

The formulation we use is borrowed from [*Stellingwerf and Wingate*, 1992; *Benz and Asphaug*, 1995]. The equation of mass conservation

$$\frac{d\rho}{} + \rho \frac{\partial v^\alpha}{} = 0 \tag{12}$$

where v is the local velocity along α, gives after SPH discretization

$$\frac{d\rho_i}{dt} = \sum_{j=1}^{N} m_j (v_i^\alpha - v_j^\alpha)\ \nabla_i^\alpha W_{ij}\ . \tag{13}$$

The equation of momemtum conservation (neglecting gravity)

$$\frac{dv^\alpha}{dt} = \frac{1}{\rho}\frac{\partial \sigma^{\alpha\beta}}{\partial x^\beta}\ , \tag{14}$$

where $\sigma^{\alpha\beta}$ is the stress tensor defined by

$$\sigma^{\alpha\beta} = -P\delta^{\alpha\beta} + S^{\alpha\beta} \tag{15}$$

where P is the pressure, $S^{\alpha\beta}$ is the deviatoric stress tensor with zero trace, and $\delta^{\alpha\beta}$ is the Kronecker symbol, becomes

$$\frac{dv_i^\alpha}{dt} = \sum_{j=1}^{N} m_j \left(\frac{\sigma_i^{\alpha\beta}}{\rho_i^2} + \frac{\sigma_j^{\alpha\beta}}{\rho_j^2}\right) \nabla_i^\beta W_{ij}\ , \tag{16}$$

written in a symmetric form. It is easy to check that the total momemtum is conserved by multiplying this equation by m_i and verifying the exact symmetry in i and j.

The equation of energy conservation

$$\frac{du}{dt} = -\frac{P}{\rho}\frac{\partial v^\alpha}{\partial x^\alpha} + \frac{1}{\rho} S^{\alpha\beta}\ \dot{\epsilon}^{\alpha\beta}\quad , \tag{17}$$

where $\dot{\epsilon}^{\alpha\beta}$ is the tensor of the rate of deformations defined by

$$\dot{\epsilon}^{\alpha\beta} = \frac{1}{2}\left(\frac{\partial v^\alpha}{\partial x^\beta} + \frac{\partial v^\beta}{\partial x^\alpha}\right)\ , \tag{18}$$

becomes

$$\frac{du_i}{dt} = \sum_{j=1}^{N} m_j (v_j^\alpha - v_i^\alpha) \left(\frac{\sigma_i^{\alpha\beta}}{\rho_i^2}\right) \nabla_i^\beta W_{ij}\ . \tag{19}$$

This symmetric form ensures an exact energy conservation.

The discretized expression of the deformation rate tensor is

$$\dot{\epsilon}_i^{\alpha\beta} = \frac{1}{2}\sum_{j=1}^{N} \frac{m_j}{\rho_j}\left((v_j^\alpha - v_i^\alpha)\nabla_i^\beta W_{ij} + (v_j^\beta - v_i^\beta)\nabla_i^\alpha W_{ij}\right)\ . \tag{20}$$

Thus

$$\begin{aligned}
\dot{\epsilon}_{xx} &= \sum_j \frac{m_j}{\rho_j}(v_j - v_i)\frac{\partial W_{ij}}{\partial x_i} \\
\dot{\epsilon}_{xy} &= \frac{1}{2}\left(\sum_j \frac{m_j}{\rho_j}(v_j^x - v_i^x)\frac{\partial W_{ij}}{\partial x_i} + \sum_j \frac{m_j}{\rho_j}(v_j^y - v_i^y)\frac{\partial W_{ij}}{\partial y_i}\right)\ ,
\end{aligned} \tag{21}$$

and similarly for $\dot{\epsilon}_{yy}$, $\dot{\epsilon}_{yx}$ and $\dot{\epsilon}_{zz}$

2.4 Deformation model

The model of mechanical deformation that we implement is the simplest possible, namely a perfect elastic-plastic model, obeying Hooke's law in the elastic regime and a suitable plasticity criterion. In the results presented in this paper, we will not reach the regime where plasticity appears and leave the study of this regime for future work. In the elastic regime, the stress tensor reads

$$\frac{dS^{\alpha\beta}}{dt} = 2\mu(\dot{\epsilon}^{\alpha\beta} - \frac{1}{3}\delta^{\alpha\beta}\ \dot{\epsilon}^{\gamma\gamma}) + S^{\alpha\gamma}R^{\beta\gamma} + S^{\gamma\beta}R^{\alpha\gamma} \tag{22}$$

where μ is the shear modulus of the material and R is the tensor of stress rotations defined by

$$R^{\alpha\beta} = \frac{1}{2}\left(\frac{\partial v^{\alpha}}{\partial x^{\beta}} - \frac{\partial v^{\beta}}{\partial x^{\alpha}}\right) \ . \tag{23}$$

Its discrete SPH approximation is similar to that of the deformation rate tensor

$$R_i^{\alpha\beta} = \frac{1}{2}\sum_{j=1}^{N}\frac{m_j}{\rho_j}\left((v_j^{\alpha} - v_i^{\alpha})\nabla_i^{\beta}W_{ij} - (v_j^{\beta} - v_i^{\beta})\nabla_i^{\alpha}W_{ij}\right) \ . \tag{24}$$

We need in addition to specify the equation of state, namely the dependence of the pressure $P = P(\rho, u)$ as a function of the density ρ and the internal energy u. We use the equation of state due to Tillotson [*Tillotson*, 1962; *Benz et al.*, 1994], which works both for expanded as well as condensed phases under large pressure or impacts. This brings in the possibility to study the effect of melting or other extreme conditions that could occur locally under conditions of fast slipping rates. We will not fully exploit this possibility in the preliminary results presented below. We do find a local temperature rise at the level of boundary particles under friction but which is insufficient to lead to melting. We thus do not incorporate the physics of thermal diffusion and the effect of the internal energy is negligible in the regime of our simulations. The parameters used in our simulations are obtained from [*Asphaug and Melosh*, 1993] for typical geological rocks, such as granite, basalt and sandstone. Their densities are respectively 2.7 $g\ cm^{-3}$ for granite and basalt and 2.3 $g\ cm^{-3}$ for sandstone. We have not observed significant differences in the solid friction for these different materials.

2.5 Geometry and scaling of the numerical experiments

We consider the classical friction experiment in which a block of mass M in contact with a solid substrate is submitted to a normal pressure P and to a constant horizontal velocity v (see figure 1). We have worked with a block of size $0.5 \times 0.375 \times 0.25\ cm^3$ while the substrate has dimension $1 \times 0.5 \times 0.25\ cm^3$. Three codes are dedicated to the construction and positionning of the block and substrate. The first code constructs the objects as ensembles of particles. The second code chisels the boundaries of the block and substrate, their rugosities and put them in contact. The initial distance and conditions are thus determined. The third code calculates the final dimensions of the objects and retrieves the coordinates of the particles at the boundaries (first and

The particles are put on a regular lattice. We have used the cubic lattice and the compact hexagonal lattice. In our simulations, we have used between 3000 and 15000 particles, as a compromise between meshing and computation time. Figure 2 shows a configuration where the particles making up the block and substrate are represented : in this example, the total number of particles in the block is $12 \times 16 \times 20 = 1520$. Thus the size of a particle is of order 0.025 cm. A slider block of a centimeter scale can thus be viewed as being constituted of effective particles of a fraction of a millimeter. We must thus incorporate the correct physics at the scale of each particle. Each particle at the boundary can be viewed as an elementary asperity that will interact with the particle-asperities of the substrate.

Associated to their size h , mass m and interaction with neighbors, each particle has a characteristic oscillation frequency ω_0 given by

$$\omega_0 = \sqrt{\frac{K}{m}} \approx \frac{1}{h} \sqrt{\frac{E}{\rho}} \ , \tag{25}$$

where E is the Young modulus and ρ is the density of the material. We have used the fact that the effective elastic constant K felt by a particle is $K \approx h\ E$ and the mass of a particle is $m \approx \rho\ h^3$. Take $h \approx 0.025\ cm$, $E = 10^{11}\ Pa$ and $\rho \approx 3\ 10^3\ kg.cm^{-3}$, we get $\omega_0 \approx 2.3\ 10^7\ s^{-1}$ and a natural frequency $\omega_0/2\pi \approx 4\ 10^6\ s^{-1}$. The expression (25) can be written in terms of the period of oscillation

$$T_0 \equiv \frac{2\pi}{\omega_0} = 2\pi\ h\sqrt{\frac{\rho}{E}} = 2\pi\ \frac{h}{c} \approx 2.5\ 10^{-5}\ s \ , \tag{26}$$

where c is the longitudinal sound velocity. This period can be compared to the time

$$t_0 = \frac{h}{v} \tag{27}$$

it takes for a particle driven at a velocity v to move over the distance h. $t_0/T_0 = (1/2\pi)\ (v/c)$ is thus small for subsonic slider block velocities.

The boundary particles are accelerated due to their collision with the substrate under the imposed sliding velocity. Due to their acceleration, they entrain their neighbors which themselves accelerate and entrain their neighbors, and so on. Macroscopically, this is nothing but wave radiation which may act as an important damping process. Since the only physical ingredient of our model incorporates elastic interaction, friction can only emerge as a result of dissipation due to wave radiation. We thus need to estimate how the efficiency of this radiation is modified by the coarse-graining at the scale of the particles and correct for it.

Recall that a particle of mass m submitted to a force F_{ext} accelerates according to

$$m_i\ \dot{v} = F_{ext} \ . \tag{28}$$

Radiation is a generic phenomenon that reflects the acceleration of the body under consideration. Generically, the power radiated from a body accelerating at $\dot{v}$ is proportional to the square of its acceleration

$$P(t) = mT_0\ \dot{v}^2 \ . \tag{29}$$

Note that this result holds not only for acoustic waves, but for any wave (electromagnetic, gravitational, hydrodynamics, etc). This radiation exerts a feedback force F_{rad} that modifies the acceleration of the body as follows [*Jackson*, 1962]. Assuming the existence of this radiation force, we replace (28) by

$$m\ \dot{v} = F_{ext} + F_{rad}\ . \tag{30}$$

F_{rad} is determined from the condition that its work during $t_1 < t < t_2$ is equal to the radiation energy

$$\int_{t_1}^{t_2} F_{rad} \cdot v dt = -\int_{t_1}^{t_2} mT_0\ \dot{v}^2\ dt\ . \tag{31}$$

Integrating by part, we get

$$\int_{t_1}^{t_2} F_{rad} \cdot v dt = mT_0 \int_{t_1}^{t_2} \ddot{v} \cdot \dot{v}\ dt - mT_0(\dot{v}\cdot v)\Big]_{t_1}^{t_2}\ . \tag{32}$$

For a periodic motion or if $(\dot{v}\cdot v) = 0$ at $t = t_1$ and $t = t_2$,

$$\int_{t_1}^{t_2} (F_{rad} - mT_0\ \ddot{v}) \cdot v dt = 0\ , \tag{33}$$

thus leading to

$$F_{rad} = mT_0\ \ddot{v}\ \ . \tag{34}$$

This effective force is indeed a dissipation as its sign changes under time reversal $t \to -t$: recall that dissipation is nothing but the lack of invariance of the motion with respect to the change $t \to -t$. The important point is that the dissipation force due to radiation is proportional to the derivative of the acceleration, i.e. to the third-order derivative of the position. This is quite different from the first-order derivative dependence of standard fluid friction. The upshot is that radiation is extremely efficient at high frequencies, since its power is proportional to $\dot{v}^2$ and thus to the fourth power of the frequency, according to (29) (this is nothing but Rayleigh's scattering law for radiations from objects smaller than the wavelength, which is indeed universal as it relies solely on dimensional considerations as first derived by Rayleigh (see [*Sornette*, 1989] for a review and references therein). The problem however from our perspective is that radiation efficiency becomes very small for small frequencies. Since coarse-graining using a finite particle size decreases the natural oscillation frequencies, the resulting radiated power will be largely reduced compared to the case of a real material in which the particle sizes are the atomic scale.

To estimate this effect of coarse-graining on the radiation efficiency, we take $\dot{v} = A\omega_0^2$ with the typical amplitude of motion given by $A = h\ \epsilon$. A reasonable estimation of the strain ϵ is such that the elastic potential energy stored per unit volume $(1/2)\sigma\epsilon$ be equal to the kinetic energy density $(1/2)\rho v^2$. This leads to $\epsilon = v\ \sqrt{\rho/E}$ and thus $A = h\ v\ \sqrt{\rho/E}$. Inserting in (29), we find that the radiated power per particle is $P = 2\pi\ \sqrt{\rho\ E}\ v^2\ h^2$. Physically, the important quantity to establish the energy balance and the friction law is the radiated energy per unit volume

$$P/h^3 = 2\pi\ \sqrt{\rho\ E}\ \frac{v^2}{\ } \tag{35}$$

Since h is about 10^5 larger than the atomic scale, the radiation efficiency in our coarse-grained formulation stemming from the acceleration of the SPH particles may be down to 10^{-5} that of expected physical one. This implies that we need to add a dissipation term to the equation in each particle to account for the physical radiation due to the accelerations at the sub-particle scale that is not correctly described by the coarse-graining at the particle scale. Our hypothesis, that will be confirmed below, is that friction is not sensitive to the specific form of the internal dissipation as long as it is present to damp out the vibrations.

2.6 Dissipation

Friction is fundamentally about dissipation. As we already mentionned, this dissipation can be in the form of radiated waves or conversion of local vibrations (phonons) into others modes, thus corresponding to an effective loss of energy. To be consistent with our preceding discussion, we need to add a dissipation term in the equation of motion proportional to the derivative of the acceleration. We would however need to scale the amplitude of this term by a factor up to 10^5 in order to obtain a correct scaling of the radiation power at the characteristic particle frequency. The problem however is that a much larger spectrum of frequencies are excited in the complex sliding motion and it is not possible to scale simultaneously the radiation at all these frequencies simultaneously. We have prefered a simpler approach which is to add a standard viscous dissipation force on each particle

$$f_{diss} = -m\gamma v \ , \tag{36}$$

with a viscous coefficient which is a parameter of the model. Here, v is the velocity of a particle with respect to the center of mass of the slider block. As a consequence, this viscous dissipation acting within each particle damps their motion and thus converts a part of the sliding kinetic energy into losses that will finally produce the solid friction behavior. We have varied γ in the interval between 0 and 10^{10} s^{-1}. Consistent with the use of this term (36) as a device to mimick losses from radiation processes, we have not included this term in the energy balance equation. In other words, any heat produced by this dissipation is assumed to be instantaneously radiated.

Before resorting to this viscous dissipation, we have explored various other possibilities, such as trapping the acoustic waves in dissipative cavities of various form, so as to mimick out-going escaping radiated waves that never come back. Unfortunately, in addition to the partial backscattering occuring at junctions (even with our best effort to adapt the acoustic impedance by using smooth geometries and slowly varying mechanical properties), we found that the pattern of the acoustic particle vibrations self-organized so that the amplitude became vanishing small at the borders of these traps, making them totally inefficient. Recall that during a typical experiment of one millisecond at 10 m/s, the slider block slips over 1 cm while the acoustic vibrations propagate over about 5 m, i.e. have time to make 5000 travels back and forth within the slider block. There is a lot of shaking and organization of particle vibration going on all the time!

From a numerical point of view, it is also necessary to incorporate a numerical viscosity that allows to regularize large gradients as occur for instance in shocks. This

artificial viscosity modifies the equation of momentum conservation into

$$\frac{dv_i^\alpha}{dt} = \sum_{j=1}^{N} m_j \left(\frac{\sigma_i^{\alpha\beta}}{\rho_i^2} + \frac{\sigma_j^{\alpha\beta}}{\rho_j^2} + \Pi_{ij} \right) \nabla_i^\beta W_{ij} \ . \tag{37}$$

Correspondingly, the artificial viscosity also brings in a contribution to the equation of energy conservation. The addition term is similar to a pressure

$$\Pi_{ij} = \begin{cases} \frac{-\alpha \overline{c}_{ij} \mu_{ij} + \beta \mu_{ij}^2}{\overline{\rho}_{ij}} & \text{if } (\vec{v}_i - \vec{v}_j) \cdot (\vec{r}_i - \vec{r}_j) \leq 0 \\ 0 & \text{else} \ , \end{cases} \tag{38}$$

where $\overline{c}_{ij} = \frac{1}{2}(c_i + c_j)$ and c_i and c_j are the sound velocities in the particles i and j. The average density is defined by $\overline{\rho}_{ij} = \frac{1}{2}(\rho_i + \rho_j)$. The estimation of the divergence of the relative velocity between i et j is

$$\mu_{ij} = \frac{h(\vec{v}_i - \vec{v}_j) \cdot (\vec{r}_i - \vec{r}_j)}{|\vec{r}_i - \vec{r}_j|^2 + \epsilon h^2} \ . \tag{39}$$

The addition term ϵh^2 prevents a divergence occurring for small $|\vec{r}_i - \vec{r}_j|$. For instance, the choice $\epsilon = 0.01$ gives a correct smoothing of the velocity only if the interparticle distance is larger than $0.1h$.

Note that Π_{ij} remains symmetric in i and j which ensures the conservation of the total linear and angular momenta. The artificial viscosity disappears when the two particles separate, which ensures that this dissipation obeys the second law of thermodynamics, i.e. can only increase the entropy of the system. The values of the parameters α and β are not critical. In the following, we adopt $\alpha = 1$ and $\beta = 0.1$. We have checked that the additional "dissipation" stemming from rounding and integrating errors is negligible.

This artificial viscosity introduced in the SPH formulation may produce a non-negligible dissipation when shear is important and we have been concerned with the possibility that the effects reported below could stem purely from numerical effects. We believe that the artificial viscosity does not produce in itself a solid friction from three observations :

- the relative velocities of the particles with respect to the center of mass are small ;
- the solid friction coefficient is zero, to within numerical accuracy, when $\gamma = 0$, i.e. the artificial viscosity alone does not produce a detectable friction ;
- the temperature does not increase appreciably. This provides an upperbound for the dissipated energy due to the artificial viscosity (recall that the viscosity (36) is not incorporated in the heat production as mentionned above), which is thus found negligible.

We conclude that the results reported below are not the expression of numerical tuning.

2.7 Implementation

Each particle carries 13 variables : three positions (x, y, z), three velocities (v_x, v_y, v_z), the density, the energy, and five components of the deviatoric stress tensor $s_{xx}, s_{yy}, s_{xy}, s_{xz}, s_{yz}$. At each time step, this set of 13 variables is incremented. The temporal integration is carried out using a second order Runge-Kunta-Fehlberg algorithm with adaptative time steps. To ensure second order accuracy, the forces are evaluated twice per time step. When a particle is suddenly colliding with another one, the local stress can jump to high values resulting in a drastic reduction of the time step reaching in some cases a factor 100! The typical time step is $5\ 10^{-8}$ seconds. Our simulations are run over $20,000$ to $50,000$ time steps, i.e. over a total duration of a millisecond or more. The simulations have been performed on RISK6000 and Ultra-Sparc 2 workstations and typically last three days.

Starting from a configuration where the block is in contact with the substrate, at a distance equal to the inter-particle spacing, we submit the block to a vertical normal pressure along the z axis. This is done by applying the same force on all the particles on the upper boundary of the block. The bottom boundary of the substrate is fixed and cannot move. The pressure is applied progressively as $1-\exp(-t/\tau)$, with a characteristic $\tau \approx 30 - 250\ \mu s$, which is not too short to allow for the propagation of acoustic waves back and for the system to reach mechanical equilibrium. We have varied the pressure from $10^6\ Pa$ to $10^9\ Pa$. Once the equilibrium is —bf reached, we impose a horizontal sliding velocity v. This velocity was varied v in the range 0.1 to 10 m/s. During the first integration time step, all particle in the sliding block are moved with velocity v. During the rest of the integration, only those particles in the first and sometimes second layers of the sliding block are moved with velocity v the others ones evolving according to the laws of elasticity. This somewhat cumbersome starting procedure prevents large unwanted inertial oscillations to occur that would require a long time to damp and brings the slider block efficiently to a constant velocity. Our choice to push the sliding block at its upper boundary is an attempt to mimick large scale driving boundary conditions. It also allows the block to freely adjust itself close to the interface with the substrate in the hope to minimize the influence of boundary conditions.

At each time step, the forces exerted on each particle are calculated. They are the cohesion force f_{coh} between each particle, the uniaxial pressure f_{pb} exerted at the upper boundary of the slider block, the repulsion force f_{spr} at the block-substrate interface that acts only between the particles in the first layer of each objects, the viscous dissipation force $f_{dis} = -\gamma(v_x - v)$ along the x-axis, and $-\gamma v_y$ along the y-axis and $-\gamma v_z$ along the z-axis. The conservation of momentum reads

$$m\ \dot{v} = f_{coh} + f_{pb} + f_{spr} + f_{dis}\ . \tag{40}$$

The solid friction force is measured as the force f^x_{spr} exerted along the direction of motion Ox by the substrate on the particles in the first layer of the slider block in contact with the substrate. We also measure the vertical component and the ratio

$$\mu \equiv f^x_{spr}/f^z_{spr} \tag{41}$$

gives a local and instantaneous measure of the solid friction coefficient. We can then perform a time average and space average to get the macroscopic friction coefficient.

We have investigated several types of boundary forces between substrate and slider block particles :

1. spring-like force

$$f_1(r) = \begin{cases} -K(r-h) & 0 < r < h \\ 0 & r > h \end{cases} \tag{42}$$

2. Smooth repulsive force [*Monaghan*, 1994]

$$f_2(r) = \begin{cases} A(\frac{l}{r})^s & 0 < r < l \\ D(r-b)^2 & l < r < b \\ 0 & r > b \end{cases} \tag{43}$$

This force is also radial and its first derivative is continuous. The continuity condition at $r = l$ gives $D = A(\frac{s+2}{2b})^2$ and $l = \frac{sb}{(s+2)}$. In our calculations, we take $b = h$.

3. Lennard-Jones force per unit of mass

$$f_3(r) = \begin{cases} \epsilon\left((\frac{l}{r})^m - (\frac{l}{r})^n\right) & 0 < r < r_c \quad \text{with } m > n \\ A(R-r)^2 + D(R-r) & r_c < r < R \\ 0 & r > R \end{cases} \tag{44}$$

$f_3(r)$ vanishes for $r = l$ and $r = R$ and has a minimum at $r = r_c$. In our simulations, we have taken $R = \frac{3}{2}\Delta p$ and $l = \Delta p$. The continuity of $f_3(r)$ and of its first derivative at $r = r_c$ implies

$$l = r_c \left(\frac{n}{m}\right)^{\frac{1}{m-n}} \tag{45}$$

and

$$A = -\frac{D}{2(R - r_c)} \ , \tag{46}$$

from which we derive

$$D = \frac{2\epsilon}{R - r_c}\left[\left(\frac{n}{m}\right)^{\frac{m}{m-n}} - \left(\frac{n}{m}\right)^{\frac{n}{m-n}}\right] \ . \tag{47}$$

ϵ remains an adjustable parameter that is chosen so that the time scale

$$\delta t = \frac{1}{2}\frac{h}{c_s} \ . \tag{48}$$

With $\Delta p = h$, this leads to

$$\epsilon = \frac{4}{9}\frac{c_s^2}{h}\left(\frac{n}{m}\right)^{\frac{1}{m-n}} \frac{1}{m-n} \tag{49}$$

We have used $m = 8, n = 4$ and $m = 12, n = 6$ and found no significant difference in the results.

Even without introducing asperities explicit, the potential field seen by particles at the interface between substrate and slider block is not smooth. Due to the particle structure, the potential thus exhibits a periodic structure of troughs and peaks with a period equal to that of the cubic or hexagonal lattice used to construct the block and substrate. This corresponds to a slider block with a periodically modulated roughness sliding on a substrate presenting also a periodically modulated roughness. We have also investigated cases for which we explicitly introduced random asperities.

3 Solid friction for periodic roughness

3.1 Measurements

We have carried out simulations for various dissipation coefficient γ. Figure 3a shows the local friction coefficient $\mu \equiv f^x_{spr}/f^z_{spr}$ as defined in (41) measured on a single particle in the first layer of the slider block in contact with the substrate. The simulation uses the boundary force f_1 defined by (42). The total number of particles used is 5504, the sliding velocity $v = 1\ m/s$, the applied pressure 10^8 Pa, and the dissipation parameters $\alpha = 0.1, \gamma = 10^6\ s^{-1}$. The positive and negative oscillations correspond to alternative braking and accelerating phases of the particle as it climbs up and down the asperities of the substrate. The time average of this local instantaneous friction coefficient is $\mu \approx -0.05$, the negative sign corresponding to a net drag. Figure 3b shows the global instantaneous friction μ_l, obtained by taking the ratio of the total force along x on all block particles on the boundary in contact with the substrate to the total force along z. We obtain the same estimate $\mu_l \approx -0.05$ for the friction coefficient after time averaging.

The following table summarizes our results for the effective friction coefficient for three different values of the dissipation γ. The simulations have otherwise been carried out exactly in the same way, using 5504 particles, an imposed sliding velocity of 1 m/s and an applied pressure of $10^8\ Pa$. In the Table, $\delta\mu$ denotes the standard deviation of μ, i.e. the amplitude of its fluctuations

α	0	0,1	0,1
γ	0	0	10^6
μ	-0.020	-0.016	-0.058
$\delta\mu$	0.017	0.017	0.007
μ_l	-0.021	-0.031	-0.050

These results are compatible with a vanishing average friction in absence of internal dissipation. When internal friction is present, the erratic motions of the particles submitted to damped multiple acoustic paths decrease somewhat and produce a finite friction coefficient which is significantly smaller than the instantaneous fluctuations. Interestingly, the value of of the friction coefficient does not appear to change with increasing γ. Above $\gamma = 10^9\ s^{-1}$, the numerical time step becomes so small making the calculation almost impossible and thus preventing us from studying this regime. For $\gamma < 10^6\ s^{-1}$, the fluctuations are too great to allow for accurate measurements. To summarize, we obtain

$$\mu \approx \mu_l \simeq -0.06 \pm 0.01 \qquad \text{for } 10^6\ s^{-1} < \gamma < 10^9\ s^{-1} \tag{50}$$

This result justifies a posteriori our procedure to model the radiation damping by the viscous dissipation (36). The remarkable fact that the solid friction coefficient is independent by and large of the amplitude of damping suggests the following picture: in the elastic regime we explore, solid friction stems from the acceleration of asperities brought in contact and collision that radiates high-frequency vibrational waves subsequently damped out, thus converting a part of the kinetic energy of the slider block into dissipation. The specific form of the internal dissipation seems not to be important, as long as there is a dissipation that can damp out the vibrations of the asperities.

3.2 Particle motions

Figure 4 shows the vertical motion of a particle of the slider block in the layer in contact with the substrate, using the boundary force f_1, 5504 particles, $v = 1\ m/s$, a pressure of $10^8\ Pa$, $\alpha = 0.1, \gamma = 10^6\ s^{-1}$. The climb and fall over the particle-asperities of the substrate are clearly visible. The downward drift is caused by a steady horizontal drift of the slider block along the y direction, perpendicular to the driving velocity. The horizontal motion of such a typical particle is almost steadily increasing, with however a short stop just when the particle is at the bottom of the potential created by the substrate asperities.

Figure 5 shows the velocity along x (fig. 5a) and along z (fig.5b) of the center of mass of the slider block, under the same conditions as described in figure 4. This shows that the slider block as a whole moves up and down as well as periodically accelerates and decelerates due to the interactions with the periodic array of asperities of the substrate.

For small $\gamma \sim 10^6\ s^{-1}$, the slider block exhibits rather large vertical oscillations that decrease significantly in amplitude as γ increases. For the largest explored γ, the slider block follows very closely the geometry of the substrate asperities. Note that the motion of a particle in the layer in contact with the substrate is a very good proxy for the motion of the slider block as a whole.

3.3 Pressure and velocity dependence

For pressure below $10^7\ Pa$, we are unable to measure a non-zero friction coefficient. Independently of the dissipation level γ, the measured μ are within uncertainty the same with or without dissipation. The reason is that the asperities do not much penetrate into each other and the slider block "floats" over the substrate without generating significant vibrations that can be dissipated. While more simulations are required to demonstrate it, we surmise that this behavior is due to the existence in the elastic regime of a critical pressure threshold below which there is zero friction.

For pressure above $10^9\ Pa$, the substrate force f_1 cannot be used anymore as the slider block penetrates within the substrate. We have then used f_2 and f_3 given by (42) and (42) respectively. Unfortunately, the integration time step shrinks drastically, thus limiting an exhaustive exploration of this regime. However, we have found that the results are the same for a pressure of $10^9\ Pa$ as found for $10^8\ Pa$. We have also verified that the three different forces give the same results.

With respect to the velocity dependence, our time-explicit numerical SPH method does not allow us to explore too *small* velocities due to the prohibitive calculation time. A few runs at $v = 0.1\ m/s$ give essentially the same results as for $v = 1\ m/s$. However, for larger velocities $v = 10\, m/s$, the friction coefficient increases and doubles at $\mu = 0.11$. The instantaneous value fluctuates with much larger amplitudes as a result of a very high level of vibrational excitations induced by the collision between asperities. The corresponding instantaneous friction coefficient measured on all the particles in the boundary layer in contact with the substrate is shown in figure 6. The simulation uses the boundary force f_1 and has 5504 particles. The parameters are $v = 10\ m/s$, which was imposed at $t = 0.2\ ms$, a pressure of $10^8\ Pa$ and dissipation $\alpha = 0, 1, \gamma = 10^6\ s^{-1}$. Note the existence of flat steps in the graph at the value $\mu = 0$: they correspond to jumps of the slider block over the substrate asperities. In these regimes, the slider block is literally flying over the substrate, as a result of an efficient transformation of horizontal to vertical momentum induced by the collisions with the substrate asperities. This regime has been postulated first by Lomnitz-Adler [1991] and our simulations confirm nicely his ideas. As a result of these jumps, the landing of the slider block does not occur in phase with the substrate. As a consequence, the evolution becomes chaotic, in the rigorous mathematical meaning of the term. The mechanism for this chaotic behavio is similar to that in the toy model of a bouncing ball on a sinusoidally vibrating table [*Mehta and Luck*, 1990; 1993; *Franaszek and Isomaki*, 1991; *Luo and Han*, 1996; *de Oliveira and Goncalves*, 1997]. The jump of the slider block occurs from roughly the maximum of the potential created by the substrate asperities and over its descent, i.e. in the pulling portion of the potential. This explains why the total time average friction coefficient is stronger as the pulling part as become weaker. We have not push more the numerical exploration of this very interesting behavior and leave it to a future publication. We expect even more interesting behavior at still larger velocities as the jump can carry the slider block over two or more asperities leading to the possibility of a rich phenomenology for the friction coefficient at these high sliding velocities.

To summarize, the main result of our investigation of the velocity dependence of the solid friction coefficient is that it *increases* at large velocities. This is in agreement with the expectation that the vibrational radiation damping becomes the dominating mechanism with an efficiency that increases fast with the velocity.

4 Disordered and fractal interfaces

We have investigated three types of disordered roughness : incommensurate periodic roughness between the block and substrate, a step and random roughnesses.

4.1 Commensurate periodic roughness

Nothing changes compared to the previous periodic case, except for the fact that we tilt the lattice structure of the slider block with respect to the substrate by an angle between 0 (previous case) and 45 degrees. When the angle is non zero, the asperities of the slider block do not encounter those of the substrate in the same configuration and at the same time. We find that, for most angles, the friction coefficient is slightly

decreased compared to the value 0.06 of the periodic case. We find a remarkable result only for the special case of the most incommensurate regime where the ratio of the mesh size of the slider block to that of the substrate lattice is equal to the golden mean $(\sqrt{5}+1)/2 \approx 1.618$. Recall that the golden mean is the irrational number that is the least well approximated by a rational number. For this ratio, no two asperities of the slider block will be in the same configuration at the same time with respect to an asperity of the substrate. The measured friction coefficient at $v = 1\ m/s$, a normal pressure of $10^8\ Pa$ and $\gamma = 10^6\ s^{-1}$ is extremely small : $\mu_l = -0.003$. Qualitatively, we attribute this small value to the conjunction of two effects. First, the tuning of the vibrational resonances occurring in the perfect periodic case does not occur anymore. This leads to much smaller coherent vibrations and thus smaller damping. Secondly, the still regular smooth roughness does not produce large local amplitudes of vibrations. We are nevertheless surprised that these effects contribute to such a small value of μ_l. Our result is reminiscent of the "super-lubrification" regime found recently [*Hirano et al.*, 1997] using a tungsten $W_{(011)}$ wire sliding over a silicium $Si_{(001)}$ surface in an incommensurate geometry and also over solid MoS_2 solid films [*Martin et al.*, 1993].

4.2 Step-like roughness

The substrate is made of a "smooth" periodic surface up to some fixed x_{step}, at which a vertical step equal to the particle size h is made by adding a single particle layer beyond x_{step}. The simulations are performed as before. The slider block is accelerated at v before the step. The simulations use the substrate force f_1, 5328 particles forming cubic lattices. Figure 7 corresponds to $v = 1\ m/s$ and a normal pressure of $10^6\ Pa$. The arrows represent the instantaneous velocities of the particle. Figure 7a shows a snapshot exactly at the time when the slider block encounters the step. Figure 7b shows that the slider block is ejected vertically and starts to jump over the step. Figure 8 corresponds to $v = 10\ m/s$ and a normal pressure of $10^8\ Pa$. It shows a latter stage when the slider block is in flight above the substrate. The arrows now show the stress carried by each particle projected in the 2D (x, z) plane. As the slider block flies over the substrate, the stress within it relaxes to zero. Its landing occurs several particles after the step and the slider block is found to bounce back several time before resumming its steady state sliding. These simulations demonstrate again the importance of jumps at high velocities, even in the presence of strong confining pressure.

4.3 Random roughnesses

Three types of randomness have been investigated: holes in the first layer of the substrate, variable heights of the substrate particles in the first layer and fractal roughness.

4.3.1 Holes in the first layer of the substrate

One could imagine first to introduce disorder by removing at random a fraction of the particles in the first layer of the substrate in contact with the slider block, thus creating holes of varying sizes and shapes controlled by the distribution of cluster

sizes in 2D percolation [*Stauffer and Aharony*, 1994]. It turns out that, for a density of holes no larger than 60 %, this has no effect on the slider block as it continues to be supported by the remaining particles of the substrate. We find the same coefficient of friction as in absence of holes. Above 60 %, the slider block starts falling partly in sufficiently large holes and the regime of sliding becomes controlled by the jumps over steps as just described. This value of 60 % corresponds approximately to the concentration of holes at which the large clusters in the substrate become of size comparable to the slider block.

4.3.2 Variable heights of the substrate particles in the first layer

The substrate is now made of a single layer of particles. These particles are again positionned regularly on a lattice in the $x - y$ plane, but their vertical positions are taken randomly and uniformly between $-\Delta z/2$ and $+\Delta z/2$. The slider block is not modified. The solid friction coefficient is now measured by measuring the total force exerted on the first layer of the slider block in contact with the substrate, as the particles in the first layer of the slider block are not continuously in contact with the substrate due to its random roughness. Figure 9 shows the measured friction coefficient μ_l as a function of time for a simulation using f_1, 6640 particles forming a cubic lattice, $v = 1\ m/s$ and a normal pressure of $10^8\ Pa$. After an initial large resistance at the beginning of the slider block motion, the friction coefficient settles to a stationary regime characterized by random fluctuations still decorated by a periodic structure reflecting that of the asperities of the slider block. We find that μ_l increases with the roughness amplitude Δz of the substrate. For $\Delta z = 0.5\ h$, $\mu_l = -0.017$ and increases continuously to $\mu_l = -0.08$ for $\Delta z = h$. Surprisingly, a small roughness *decreases* the solid friction while a larger roughness increases it above its periodic roughness value 0.06. We attribute the decrease of μ_l for small Δz to the detuning of the vibrational resonances occurring in the perfect periodic case, that were at the origin of relatively large vibrational radiation and thus damping.

4.3.3 Fractal roughness

As in the previous section, the substrate is made of a single layer of particles, positionned regularly on a 2D cubic lattice in the $x - y$ plane with mesh h. Their vertical positions are determined by using the spectral synthesis method described in [*Peitgen and Saupe*, 1988] to generate a self-affine surface. We have investigated different dimensions between $D_f = 2.1$ to $D_f = 2.9$. The slider block is made of 6440 particles organized in a hexagonal compact lattice. Thus, even without the fractal vertical structure of the substrate, there is no more commensurability between the slider block and substrate. The maximum amplitude of the self-affine surface is imposed equal to h for all values of D_f. The largest wavelength that we have kept in the construction of the substrate is equal to one eighth the length of the slider block. This ensures that the slider block remains stable and does not fall or jump over steps as in the step case. Figures 10a and 10b show two fractal surfaces, respectively with $D_f = 2.3$ and $D_f = 2.8$, with the same maximum amplitude h. Figures 11a and 11b show the locii of contacts between the substrate and the slider block for the two surfaces shown in figure 10. Figure 11a, corresponding to $D_f = 2.3$, shows a larger

and more coherent contact area than figure 11b, corresponding to $D_f = 2.8$.

Figure 12 shows the variation of the solid friction coefficient μ_l as a function of D_f for simulations performed under a normal pressure of $10^8\ Pa$, $v = 1\ m/s$ and $\gamma = 10^6\ s^{-1}$. For $D_f < 2.6$, the friction coefficient is found less than that of the perfect periodic case. As for the previous case, we attribute this result to the detuning of the vibrational resonances occurring in the perfect periodic case, that were at the origin of relatively large vibrational radiation and thus damping. For $D_f > 2.6$, the friction coefficient becomes larger than that of the perfect periodic case, reflecting the transition to another regime controlled by the larger elastic distorsion of the asperities.

5 Conclusion

We have presented a new numerical model for the investigation of solid friction properties in the regime of fast relative velocities of the order of meters to tens of meters per second. We have restricted our investigation to the regime where only elastic deformations occur between the asperities at the contact between the slider block and the substrate. In this case, the only mechanism that dissipates energy and creates a non-vanishing solid friction coefficient is through the generation of vibrational radiations that are subsequently damped out, either by escaping to infinity or by a suitable internal damping process. We have examined periodic commensurate and incommensurate asperities and various types of disordered surface. In this elastic regime, we report the evidence of a transition from zero (or non-measurable) friction to a finite friction when the normal pressure increases above about $10^6\ Pa$. We find a remarkably universal value for the friction coefficient $\mu \approx 0.06$, which is independent of the internal dissipation strength over three order of magnitudes, and independent of the detailled nature of the slider block-substrate interaction. We find that disorder may either decrease or increase μ due to the competition between two effects: Disorder detunes the coherent vibrations of the asperties that occur in the periodic case, leading to weaker acoustic radiation and thus weaker damping. On the other hand, large disorder leads to stronger vibration amplitudes at local asperities and thus stronger damping. Our simulations have confirmed the existence of jumps of the slider blocks that occur over steps or asperities for the largest velocities of $10\ m/s$. We find a velocity strengthening with a doubling of the friction coefficient when the velocity increases from $1\ m/s$ to $10\ m/s$. This reflects the increasing amplitude of vibrational damping.

We leave for another a later paper the investigation of the regime where the pressure is larger and the roughness is more disordered so that the local pressure at asperities reaches the plasticity threshold. In this regime, temperature diffusion must be added to the formulation. This does not pose any conceptual difficulty and can easily be incorporated in our code. In this regime, both vibration damping and plasticity become the source of dissipation. It is probable that the friction coefficient will be found larger in this case, as often measured in macroscopic experiments that work in the regime where asperities are deformed in the plastic regime [*Dieterich and Kilgore*, 1994]. However, we still expect that jumps play an important role at the largest velocities of tens of meter per second.

We acknowledge stimulating discussions with T. Villemin and J.-P. Vila.

References

Asphaug, E. and H.J. Melosh, The stickney impact of phobos: A dynamical model, Icarus, 101, 144-164, 1993.

Asphaug, E., S.J. Ostro, R.S. Hudson, D.J. Scheeres and W. Benz, Disruption of kilometre-sized asteroids by energetic collisions, Nature, 393, N6684, 437-440, 1998.

Baumberger, T., and L. Gauthier, Creeplike relaxation at the interface between rough solids under shear, J. Phys. I France, 6, 1021-1030, 1996.

Beeler, N.M., T.E. Tullis, M.L. Blanpied and J.D. Weeks, Frictional behavior of large displacement experimental faults, J. Geophys. Res., 101, 8697-8715, 1996.

Beeler, N.M., T.E. Tullis and J.D. Weeks, The roles of time and displacement in the evolution effect in rock friction, Geophys. Res. Lett., 21, 1987-1990, 1994.

Beeman, M., W.B. Durham and S.H. Kirby, Friction of ice, J. Geophys. Res., 93, 7625-7633, 1988.

Benz, W., Smooth particle hydrodynamics: A review, The Numerical Modeling of Nonlinear Stellar Pulsations, J. Buchler, ed., 269-288, Kluwer Academic Publishers, Dordrecht, 1990.

Benz, W., W.L. Slattery and A.G.W. Cameron, The origin of the moon and the single-impact hypothesis, Icarus, 66, 515-535, 1986.

Benz, W., and E. Asphaug, Impact simulations with fracture. I- Method and tests, Icarus, 107, 98-116, 1994.

Benz, W., E. Ryan and E. Asphaug, Numerical simulations of catastrophic disruption: Recent results, In The 4th International Workshop on the Catastrophic Disruption of Small Solar System Bodies, Gubbio, Italy, 1994.

Benz, W., and E. Asphaug, Simulations of brittle solids using smooth particle hydrodynamics, Computer Physics Communications, 87, 253-265, 1995.

Benzion, Y., and J. Rice, Earthquake failure sequences along a cellular fault zone in a 3-dimensional elastic solid containing asperity and nonasperity regions, J. Geophys. Res., 93, 14109-14131, 1993.

Benzion, Y., and J. Rice, Slip patterns and earthquake populations along different classes of faults in elastic solids, J. Geophys. Res., 100, 12959-12983, 1995.

Bocquet, L., and H.J. Jensen, Phenomenological study of hysteresis in quasistatic friction, J. Physique I, 7, 1603-1625, 1997.

Bowden, F.P., and D. Tabor, The Friction and Lubrication of Solids (Oxford University Press, 1954).

Brace, W.F., Laboratory studies of stick-slip and their application to earthquakes, Tectonophysics, 14, 189-200, 1972.

Brace, W. R., and J.D. Byerlee, Stick-slip as a mechanism for earthquakes, Science, 153, N3739, 990-992, 1966.

Brune, J.N., S. Brown and P.A. Johnson, Rupture mechanism and interface separation in foam rubber models of earthquakes - A possible solution to the heat flow paradox and the paradox of large overthrusts, Tectonophysics, 218, 59-67, 1993.

Bullard, E.C., The interior of the earth, pp.57-137, in The Earth as a planet", G.P. Kuiper, ed., University of Chicago Press, 1954 (see pp. 120-121).

Byerlee, J. D., et al., Stick slip, stable sliding, and earthquakes - Effect of rock type, pressure, strain rate, and stiffness, J. Geophys. Res., 73, 6031-6037, 1968.

Caroli, C., and P. Nozières, Dry friction as a hysteretic elastic response, In Physics of Sliding Friction, Persson et Tosatti, eds., Kluwer Academic Publishers, 1996.

Caroli, C., and B. Velicky, Dry friction as an elasto-plastic response: Effect of compressive plasticity, J. Physique I, 7, 1391-1416, 1997.

Cochard, A., and Madariaga R., Dynamic faulting under rate-dependent friction, Pure and Applied Geophysic, 142, 419-445, 1994.

Coleman, C.S. and G.V. Bicknell, Jets with entrained clouds - Hydrodynamics simulations and magnetic field structure, MNRAS, 214, 337-355, 1985.

Cox, S.J.D., Velocity-dependent friction in a large direct shear experiment on gabbro, In Deformation Mechanisms, Rheology and Tectonics, Knipe et Rutter, eds., vol. 54, 63-70, Geological Society Special Publication, 1990.

de Oliveira, C.R., and P.S. Goncalves, Bifurcations and chaos for the quasiperiodic bouncing ball, Phys. Rev. E, 56, 4868-4871, 1997.

Dieterich, J.H., Time-dependent friction in rocks, J. Geophys. Res., 77, 3690-3697, 1972.

Dieterich, J.H., Time-dependent friction and the mechanics of stick-slip, Pure and Applied Geophysics, 116, 790-806, 1978.

Dieterich, J.H., Modeling of rock friction: 1. experimental results and constitutive equations, J. Geophys. Res., 84, 2161-2168, 1979.

Dieterich, J.H., Earthquake nucleation on faults with rate and state-dependent strength, Tectonophysics, 211, 115-134, 1992.

Dieterich, J., and Kilgore B.D., Direct observation of frictional constacts- New insight for state-dependent properties, Pure and Applied Geophysics, 143, 283-302, 1994.

Franaszek, M., and H.M. Isomaki, Anomalous chaotic transients and repellers of the bouncing-ball dynamics, Phys. Rev. E, 43, 4231-4236, 1991.

Gu, Y., and T.-F. Wong, Effects of loading velocity, stiffness, and inertia on the dynamics of a single degree of freedom spring-slider system, J. Geophys. Res., 96, 21677-21691, 1991.

Henyey, T.L., and G.J. Wasserburg, Heat flow near major strike-slip faults in California, J. Geophys. Res., 76, 7924-7946, 1971.

Herrmann, H.J., G. Mantica and D. Bessis, Space-filling bearings, Phys.Rev.Lett., 65, 3223-3226, 1990.

Hirano, M., K. Shinjo, R. Kaneko and Y. Murata, Observation of superlubricity by scanning tunneling microscopy, Phys. Rev. Lett., 78, 1448-1451, 1997.

Jackson, J.D., Classical electrodynamics, 2d ed., New York, Wiley, 1975.

Jensen, H.J., Y. Brechet and B. Doucot, Instabilities of an elastic chain in a random potential, J. Phys. I France, 3, 611-623, 1993.

Johansen, A., P. Dinon, C. Ellegaard, J.S. Larsen et H.H. Rugh, Dynamic phases in a spring-block system , Phys. Rev. E, 48, 4779-4790,1993.

Knopoff, L., The organization of seismicity on fault networks, Proc. Nat. Acad. Sci. USA, 93, 3830-3837, 1996.

Lachenbruch, A.H., and Sass J.H., Heat flow and energetics of the San Andreas fault zone, J. Geophys. Res., 85, 6185-6222, 1980.

Lattanzio, J.C., J.J. Monaghan, H. Pongracic and M.P. Schwarz, Interstellar cloud collisions, MNRAS, 215, 125-147, 1985.

Lomnitz-Adler, J., Model for steady state friction, J. Geophys. Res., 96, 6121-6131, 1991.

Luck, J.-M., and A. Mehta, Bouncing ball with a finite restitution - Chattering, locking and chaos, Phys. Rev. E, 48, 3988-3997, 1993.

Lucy, L.B., A numerical approach to the testing of the fission hypothesis, Astron. J., 82, 1013-1024, 1977.

Luo, A.C.J., and R.P.S. Han, The dynamics of a bouncing ball with a sinusoidally vibrating table, Nonlinear Dynamics, 10, 1-18, 1996.

Martin, J.M., C. Donnet, T. Le Mogne and T. Epicier, Superlubricity of molybdenum disulphide, Phys. Rev. B, 48, 10583-10586, 1993.

Melosh, H.J., Dynamical weakening of faults by acoustic fluidization, Nature, 379, 601-606, 1996.

Mehta, A., and J.-M. Luck, Novel temporal behavior of a nonlinear dynamical model system - The completely inelastic bouncing ball, Phys. Rev. Lett., 65, 393-396, 1990.

Monaghan, J.J., and R.A. Gingold, Shock simulation by the particle method, J. Comput. Phys., 52, 374-389, 1983.

Monaghan, J.J., An introduction to SPH, Computer Physics Communications, 48, 89-96, 1988.

Monaghan, J.J., Smooth particle hydrodynamics, Ann. Rev. Astron. Astrophys., 30, 543-574, 1992.

Monaghan, J.J., Simulating free surface flows with SPH, J. Comput. Phys., 110, 399-406, 1994.

Monaghan, J.J., Gravity currents and solitary waves, Physica D, 98, 523-533, 1996.

Monaghan, J.J., and J.C. Lattanzio, A refined particle method for astrophysical problems, Astron. Astrophys., 149, 135-143, 1985.

Monaghan, J.J., and R.J. Humble, Vortex particle methods for periodic channel flow, J. Comput. Phys., 107, 152-159, 1993.

National Research Council; The role of fluids in crustal processes, Studies in geophysics, Geophysics study committed, Commission on Geosciences, Environment and Ressources, National Academic Press, Washington D.C., 1990.

Ouillon, G., C. Castaing and D. Sornette, Hierarchical scaling of faulting, J. Geophys. Res., 101, 5477-5487, 1996.

Peitgen, H.-O., and D. Saupe, eds., The Science of Fractal Images, Springer-Verlag, 1988.

Persson, B.N.J., and E. Tosatti, eds., Physics of sliding friction, NATO ASI Series (Kluwer Academic Publishers, Dordrecht, 1996).

Pisarenko, D., and P. Mora, Velocity weakening in a dynamical model of friction, Pure and Applied Geophysics, 142, 447-466, 1994.

Rice, J.R., Spatio-temporal complexity of slip on a fault, J.Geophys.Res., 98, 9885-9907, 1993.

Ruina, A., Slip instability and state variable friction laws, J. Geophys. Res., 88, 10359-10370, 1983.

Schmittbuhl, J., J.-P. Vilotte and S. Roux, Velocity weakening friction : A renormalization approach, J. Geophys. Res., 101, 13911-13917,1996.

Shnirman, M.G., and E.M. Blanter, Self-organized criticality in a mixed hierarchical system, preprint 1998.

Scholz, C.H., Earthquakes and friction laws, Nature, 391, N6662, 37-42, 1998.

Scott D., Seismicity and stress rotation in a granular model of the brittle crust, Nature, 381, N6583, 592-595, 1996.

Shaw, B.E., Complexity in a spatially uniform continuum fault model, Geophys. Res. Lett. 21, 1983-1986, 1994.

Shaw, B.E., Frictional weakening and slip complexity in earthquake faults, J. Geophys. Res., 102, 18239-18251, 1995.

Shaw, B.E., Model quakes in the two-dimensional wave equation, J. Geophys. Res., 100, 27367-27377, 1997.

Sokoloff, J.B., Theory of dynamical friction between idealized sliding surfaces, Surf. Sci., 144; 267-272, 1984.

Sornette, D., Acoustic waves in random media: III- Experimental situations, Acustica, 67, 15-25, 1989.

Sornette, D., P. Miltenberger and C. Vanneste, Statistical physics of fault patterns self-organized by repeated earthquakes : synchronization versus self-organized criticality, in Recent Progresses in Statistical Mechanics and Quantum Field Theory, Proceedings of the conference Statistical Mechanics and Quantum Field Theory, eds. P. Bouwknegt, P. Fendley, J. Minahan, D. Nemeschansky, K. Pilch, H. Saleur and N. Warner, World Scientific, Singapore, 1995, pp .313-332.

Stauffer, D., and A. Aharony, Introduction to percolation theory, 2nd ed., London ; Bristol, PA : Taylor & Francis, 1994.

Stellingwerf, R.F. and C.A. Wingate, Impact modeling with smooth particle hydrodynamics, In 1992 Hypervelocity Impact Symposium, 1992.

Streit, J.E., Low frictional strength of upper crustal faults: A model, J. Geophys. Res., 102, 24619-24626, 1997.

Tanguy, A., and P. Nozières, First-order bifurcation landscape in a 2D geometry - The example of solid friction, J. Physique I, 6, 1251-1270, 1996.

Tanguy, A and S. Roux, Memory effects in friction over correlated surfaces, Phys. Rev. E, 55, 2166-2173, 1997.

Tillotson, J.H., Metallic Equations of State for Hypervelocity Impact, General Atomic report GA-3216, 1962.

Tsutsumi, A., and T. Shimamoto, Frictional properties of monzodiorite and gabbro during seismogenic fault motion, J. Geol. Soc. Japan, 102, 240-248, 1996.

Tsutsumi, A., and T. Shimamoto, High-velocity frictional properties of gabbro, Geophys. Res. Lett., 24, 699-702,1997.

Figure captions

Fig. 1: Classical friction experiment in which a block of mass M in contact with a solid substrate is submitted to a normal pressure P and to a constant horizontal velocity v. We have worked with a block of size $0.5 \times 0.375 \times 0.25\ cm^3$ while the substrate has dimension $1 \times 0.5 \times 0.25\ cm^3$.

Fig. 2: A configuration where the particles making up the block and substrate are represented. In this example, the total number of particles in the block is $12 \times 16 \times 20 = 1520$. The size of a particle is of order $0.025\ cm$. A slider block of a centimeter scale is constituted of effective particles of a fraction of a millimeter that act as constitutive grains. Each particle at the boundary is an elementary asperity that interacts with the particle-asperities of the substrate.

Fig. 3: a) Local friction coefficient $\mu \equiv f^x_{spr}/f^z_{spr}$ as defined in (41) measured on a single particle in the first layer of the slider block in contact with the substrate. The simulation uses the boundary force f_1 defined by (42). The total number of particles is 5504, the sliding velocity is $v = 1\ m/s$, the applied pressure is 10^8 Pa, the dissipation parameters are $\alpha = 0.1, \gamma = 10^6\ s^{-1}$. The time average of this local instantaneous friction coefficient is $\mu \approx -0.05$, the negative sign corresponding to a net drag.

b) Global instantaneous friction μ_l, obtained by taking the ratio of the total force along x on all block particles on the boundary in contact with the substrate to the total force along z. We obtain the same estimate $\mu_l \approx -0.05$ for the friction coefficient when time averaging.

Fig. 4: Vertical motion of a particle of the slider block in the layer in contact with the substrate, using the boundary force f_1, 5504 particles, $v = 1\ m/s$, a pressure of $10^8\ Pa$, $\alpha = 0.1, \gamma = 10^6\ s^{-1}$.

Fig. 5: Velocity along x (fig. 5a) and along z (fig.5b) of the center of mass of the slider block, under the same conditions as for figure 4.

Fig. 6: Instantaneous friction coefficient measured on all the particles in the boundary layer in contact with the substrate using the boundary force f_1, 5504 particles, $v = 10\ m/s$ which was imposed at $t = 2\ ms$, a pressure of $10^8\ Pa$ and dissipation $\alpha = 0, 1, \gamma = 10^6\ s^{-1}$. The flat steps in the graph at the value $\mu = 0$ correspond to jumps of the slider block over the substrate asperities.

Fig. 7: Motion of the slider block over a step of height h after having been accelerated $v = 1\ m/s$ before the step. The simulations use the substrate force f_1, 5328 particles forming cubic lattices and a normal pressure of $10^6\ Pa$. The arrows represent the instantaneous velocities of the particle.

a) Snapshot exactly at the time when the slider block encounters the step.

b) The slider block is ejected vertically and starts to jump over the step.

Fig. 8: Same as figure 7 but showing a latter time for different parameters

$v = 10\ m/s$ and a normal pressure of $10^8\ Pa$. The arrows show the stress carried by each particle projected in the 2D (x, z) plane.

Fig. 9: Measured friction coefficient μ_l as a function of time for a simulation using f_1, 6640 particles forming cubic lattices, $v = 1\ m/s$ and a normal pressure of $10^8\ Pa$. The substrate is made of a single layer of particles positionned regularly on a lattice in the $x - y$ plane, but with their vertical positions taken randomly and uniformly between $-\Delta z/2$ and $+\Delta z/2$. The slider block is not modified.

Fig. 10: Two fractal surfaces, respectively with fractal dimensions $D_f = 2.3$ (fig.10a) and $D_f = 2.8$ (fig.10b), with the same maximum amplitude equal to h. As for fig.9, the substrate is made of a single layer of particles, positionned regularly on a 2D cubic lattice in the $x - y$ plane with mesh h. Their vertical positions are determined by using the spectral synthesis method described in [*Peitgen and Saupe*, 1988] to generate a self-affine surface. The slider block is made of 6440 particles organized in a hexagonal compact lattice. The largest wavelength in the fractal surfaces is equal to one eighth the length of the slider block to ensure the stability of the slider block during its motion.

Fig. 11: Locii of contacts between the substrate and the slider block for the two surfaces shown in figure 10. Figure 11a, corresponding to $D_f = 2.3$, shows a larger and more coherent contact area than figure 11b, corresponding to $D_f = 2.8$.

Fig. 12: Variation of the solid friction coefficient μ_l as a function of the substrate fraction dimension D_f for simulations performed under a normal pressure of $10^8\ Pa$, $v = 1\ m/s$ and $\gamma = 10^6\ s^{-1}$.

This figure "fig1.gif" is available in "gif" format from:

http://arXiv.org/ps/cond-mat/9809213v1

This figure "fig2.gif" is available in "gif" format from:

http://arXiv.org/ps/cond-mat/9809213v1

This figure "fig3a.gif" is available in "gif" format from:

http://arXiv.org/ps/cond-mat/9809213v1

This figure "fig3b.gif" is available in "gif" format from:

http://arXiv.org/ps/cond-mat/9809213v1

This figure "fig4.gif" is available in "gif" format from:

http://arXiv.org/ps/cond-mat/9809213v1

This figure "fig5a.gif" is available in "gif" format from:

http://arXiv.org/ps/cond-mat/9809213v1

This figure "fig5b.gif" is available in "gif" format from:

http://arXiv.org/ps/cond-mat/9809213v1

This figure "fig6.gif" is available in "gif" format from:

http://arXiv.org/ps/cond-mat/9809213v1

This figure "fig7a.gif" is available in "gif" format from:

http://arXiv.org/ps/cond-mat/9809213v1

This figure "fig7b.gif" is available in "gif" format from:

http://arXiv.org/ps/cond-mat/9809213v1

This figure "fig8a.gif" is available in "gif" format from:

http://arXiv.org/ps/cond-mat/9809213v1

This figure "fig8b.gif" is available in "gif" format from:

http://arXiv.org/ps/cond-mat/9809213v1

This figure "fig9.gif" is available in "gif" format from:

http://arXiv.org/ps/cond-mat/9809213v1

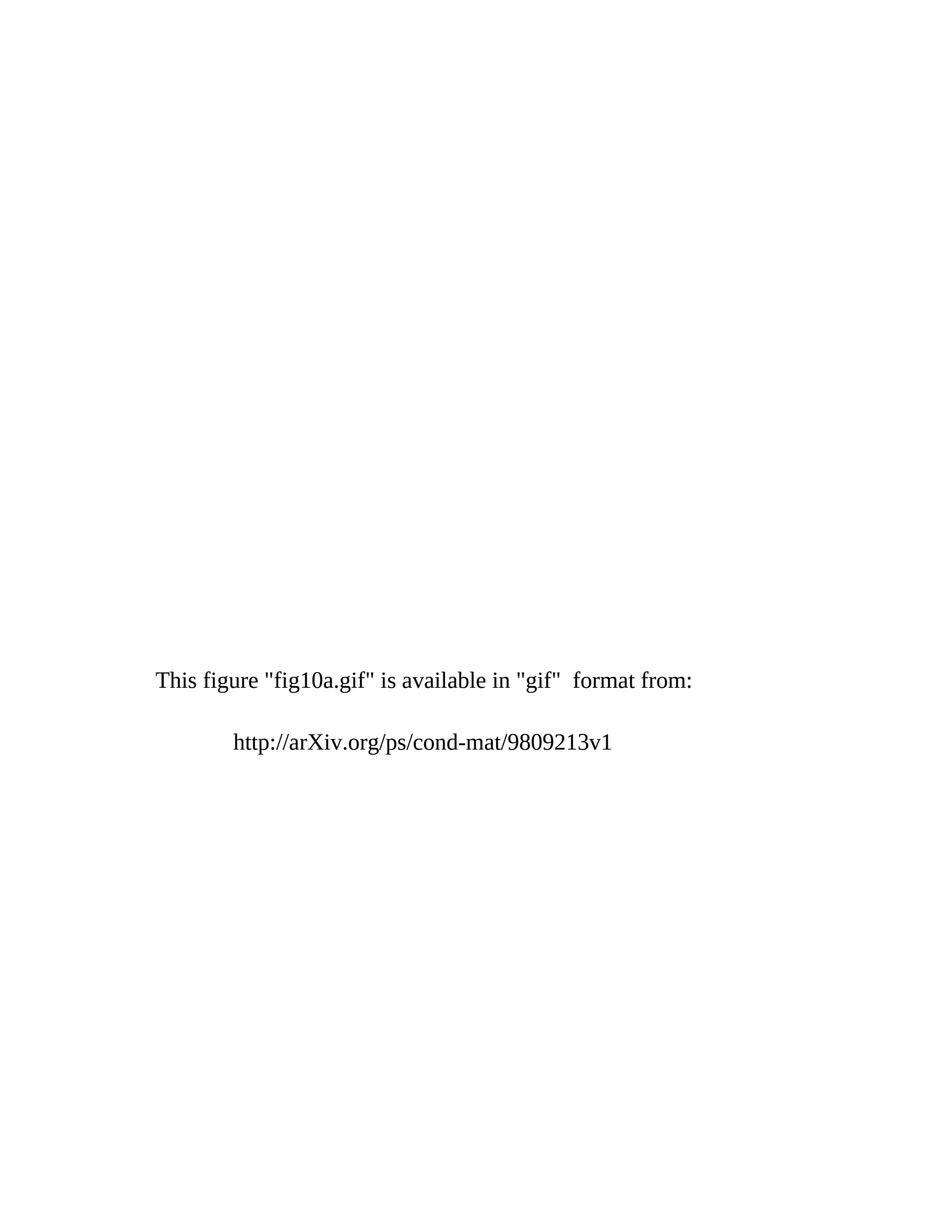
This figure "fig10a.gif" is available in "gif" format from:
http://arXiv.org/ps/cond-mat/9809213v1

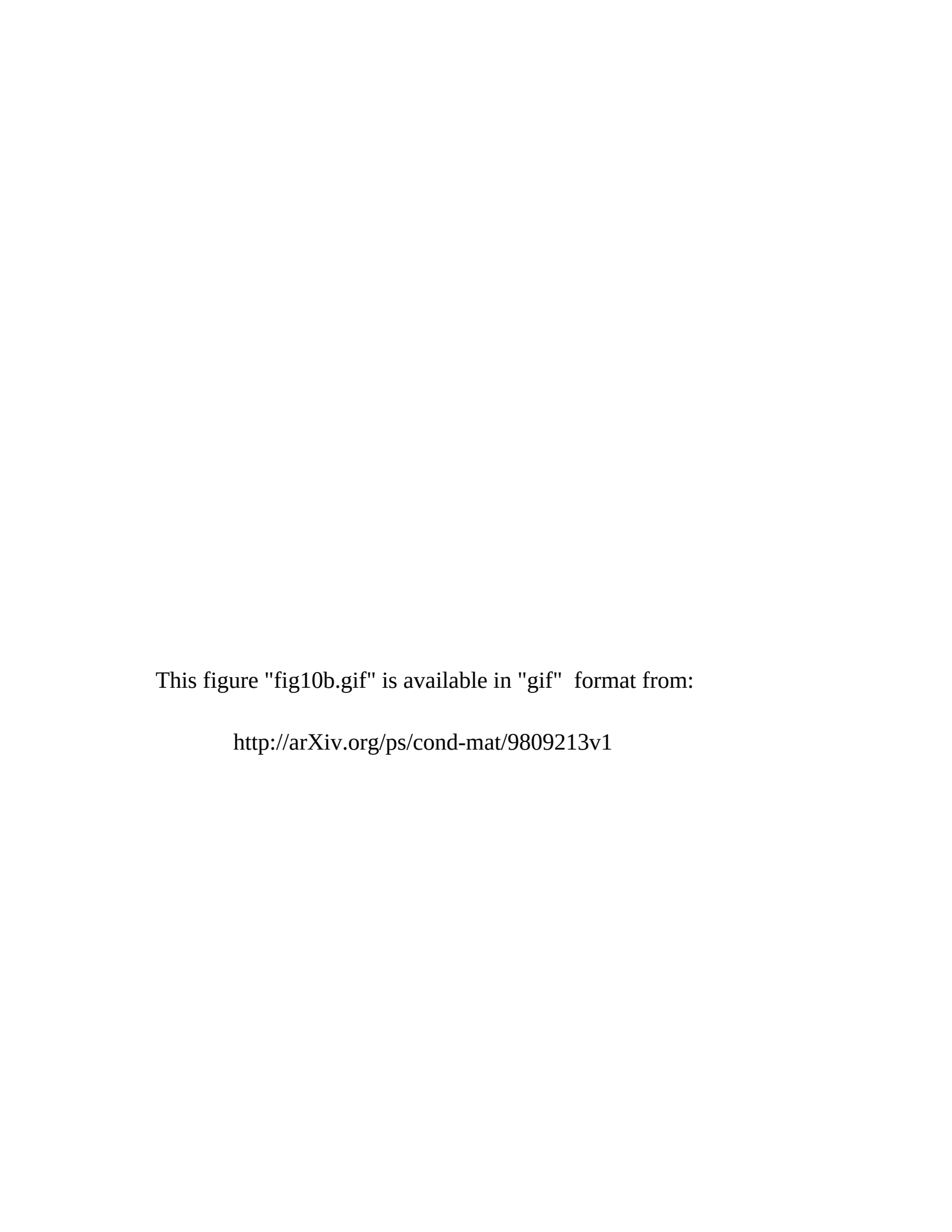
This figure "fig10b.gif" is available in "gif" format from:
http://arXiv.org/ps/cond-mat/9809213v1

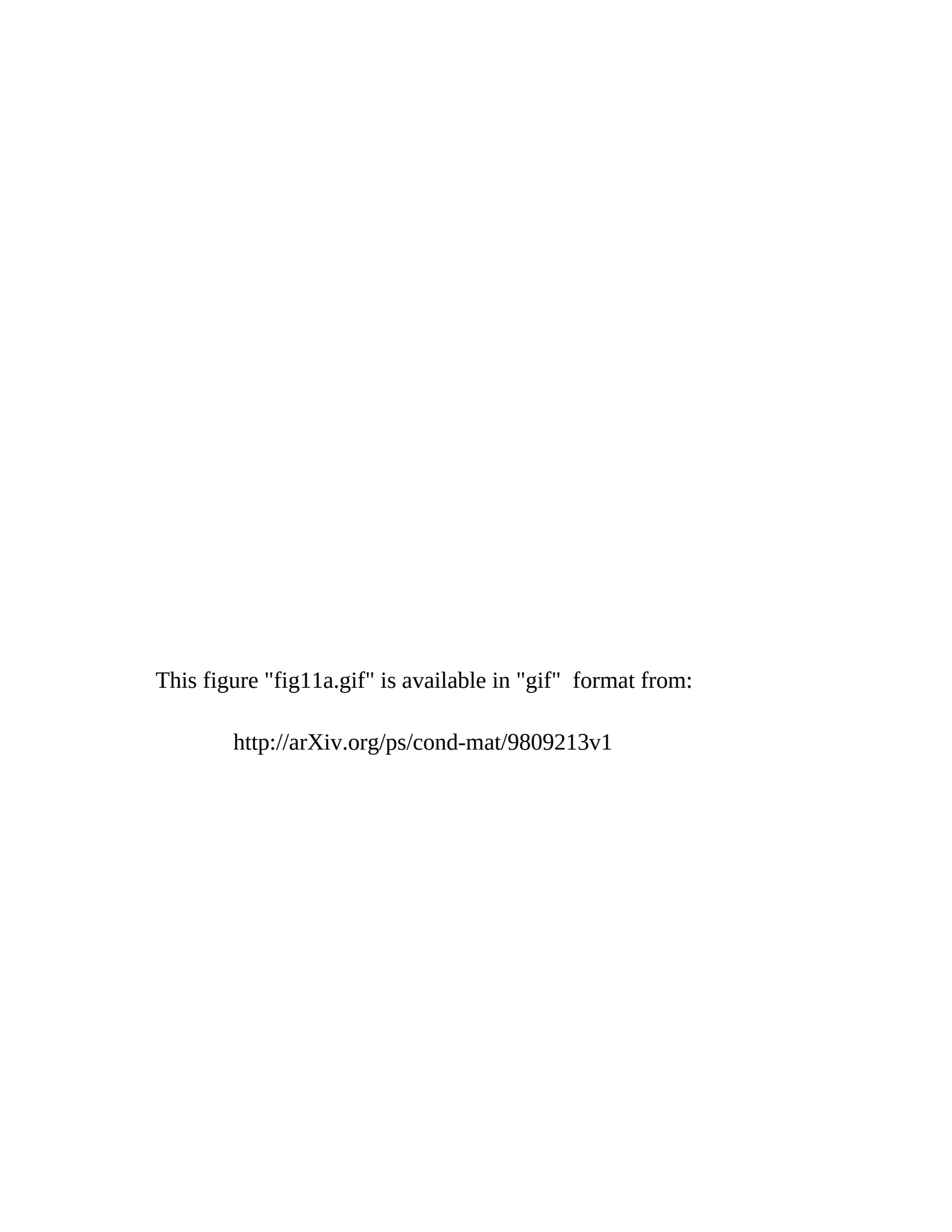
This figure "fig11a.gif" is available in "gif" format from:
http://arXiv.org/ps/cond-mat/9809213v1

This figure "fig11b.gif" is available in "gif" format from:

http://arXiv.org/ps/cond-mat/9809213v1

This figure "fig12.gif" is available in "gif" format from:

http://arXiv.org/ps/cond-mat/9809213v1